Preliminary projectile impact and safety analyses for the Hayabusa2 extended mission

Mirko Trisolini*
Politecnico di Milano, Milan, Italy

Anivid Pedros-Faura†
University of Colorado Boulder, United States

Yuichi Tsuda‡
Institute of Space and Astronautical Science / JAXA, Japan

Shota Kikuchi§
National Astronomical Observatory of Japan, Japan

This work presents the preliminary analysis of the projectile deployment by the Hayabusa2 extended mission (Hayabusa2#) after its planned rendezvous with asteroid 1998 KY26. Hayabusa2# will be the first ever mission to rendezvous with such a rapidly rotating small asteroid, posing significant engineering challenges because of its distinctive dynamical environment. In this paper, the impact cratering event is studied along with the dynamical evolution of the ejecta plume. In addition, a preliminary assessment of the risk posed by the ejecta plume during the projectile release operations is carried out.

I. Introduction

Following the successful completion of its primary mission, with the return of samples form asteroid Ryugu back to Earth on December 6, 2020, the Hayabusa2 spacecraft started a new journey towards asteroid 1998 KY26 [1–3]. The current spacecraft trajectory was designed to also include a flyby with (98943) 2001 CC21 in June 2026 followed by the arrival at 1998 KY26 scheduled for July 2031. Thus, after a 10-year interplanetary cruise [3], Hayabusa2 will start close proximity operations to characterise its last mission target.

This new target is a small, fast-rotating asteroid, with a diameter of just about 30 meters and a rotational period as small as 10.7 minutes [4]. The extended mission, Hayabusa2#, will thus be the first one to rendezvous with such a fast-rotating small asteroid, giving the opportunity to gather important scientific information on these types of bodies. Asteroid 1998 KY26 is in fact representative of small bodies below 100 meters in diameter, which are the most common in the Solar System and usually enter the Earth's atmosphere causing impacts and fireball events. Therefore, the Hayabusa2# mission can significantly enhance the knowledge of these bodies and help prevent and predict potentially hazardous events. Furthermore, close-proximity operations will pose unprecedented technical challenges serving as a valuable engineering demonstration to devise suitable operation schemes for small fast-rotators.

When Hayabusa2# rendezvous with asteroid 1998 KY26 in 2031, it will still have the possibility to deploy two payloads to perform advanced operations: a small projectile and a target marker [2, 3]. On one hand, the target marker can be used for terrain-relative navigation and gravity field estimation, thus improving the capability to model the dynamical environment of 1998 KY26 [5]. On the other hand, the projectile can be used to better characterise the physical properties of the asteroid's terrain. By releasing the projectile onto the asteroid's surface and observing its effects in terms of plume generation and crater formation, key information on the soil properties can be inferred.

In this work, we study the dynamical behaviour of the ejected fragments, following the release of the small projectile still on board. Given the limited information currently available on the physical characteristics of 1998 KY26, we perform parametric analyses, varying both the asteroid soil cohesion level and the impact location. In the first case,

*Currently Astrodynamic Specialist at Vyoma GmbH, Karl-Theodor-Str. 55, 80803, Munich, Germany.
†PhD student, University of Colorado Boulder, Boulder, CO 80309, United States. Member AIAA.
‡Professor/Hayabusa2 Project Manager, Institute of Space and Astronautical Science (ISAS)/Japan Aerospace Exploration Agency (JAXA), Sagamihara, Japan. Member AIAA.
§Assistant Professor, National Astronomical Observatory of Japan, 2-21-1 Osawa, Mitaka, Tokyo 181-8588, Japan. Member AIAA.

we assess the influence of the soil properties of 1998 KY26 on the crater formation event and subsequently on the dynamical evolution of the ejecta. In the second case, we analyse the interaction between the low-gravity dynamical environment of the asteroid and its fast rotational speed on the fate of the ejecta. Following the dynamical analysis, we also present a preliminary risk assessment for the spacecraft during the projectile release operations. In this case, we evaluate the interaction between the ejecta plume and the spacecraft for different projectile release altitudes.

II. Methodology

The methodology followed in this work is based on the combination of a dynamical model for the propagation of the trajectory of the ejected fragments, an ejecta distribution model that is used to characterise the impact cratering event and generate the initial conditions of the propagation, and Ballistic Limit Equations (BLEs) to assess the interaction between the plume and the spacecraft.

A. Dynamical Environment

The dynamical model used for all the propagation presented in this work is the Photo-gravitational Hill Problem [6, 7], including the effect of the asteroid oblateness, J_2. The equations of motion are expressed in non-dimensional form in a synodic reference frame centred at the asteroid (Eq. 1). The x-axis is along the Sun-asteroid direction, pointing outwards, the z-axis is along the direction of the angular momentum of the asteroid orbit, and the y-axis completes the right-hand coordinate system.

$$\begin{cases} \ddot{x} - 2\dot{y} = 3x + \beta + g_x \\ \ddot{y} + 2\dot{x} = g_y \\ \ddot{z} = -z + g_z \end{cases}, \tag{1}$$

where x, y, and z are the non-dimensional particle positions with respect to the centre of the asteroid in the synodic frame, $r = \sqrt{x^2 + y^2 + z^2}$ is the particle's distance from the centre of the asteroid, g_x, g_y, and g_z are the components of the gravitational acceleration of the asteroid, and β is lightness parameter, which can be expressed as:

$$\beta = \frac{P_0}{c} \frac{AU^2}{\mu_a^{1/3} \mu_{\text{Sun}}^{2/3}} \frac{3(1 + c_{\text{R}})}{2\rho_{\text{p}} d_{\text{p}}}. \tag{2}$$

Here, $P_0 = 1367\ \text{W m}^{-2}$ is the solar flux at 1 AU, c is the speed of light, AU is the astronomical unit, μ_{Sun} and μ_a are the gravitational parameters of the Sun and the asteroid, respectively, ρ_{p} is the particle density and d_{p} the particle diameter. The reflectivity coefficient, c_{R}, is a number between 0 and 1, where 1 is for fully reflective surfaces. Eclipses are taken into account using a cylindrical shadow model via a modified lightness parameter, β^* [8]:

$$\beta^* = \begin{cases} \beta & \text{if } x \leq 0 \\ \beta \cdot f(\sigma) & \text{otherwise} \end{cases}, \tag{3}$$

where $f(\sigma) = (1 + e^{-s \cdot \sigma})^{-1}$ is a sigmoid function with steepness parameter s, which, in this work is equal to 8 [8]. The variable $\sigma = r_x - R_a$, with $r_x = \sqrt{y^2 + z^2}$ distance to the x-axis, and R_a mean radius of the asteroid.

B. Ejecta Model

The ejecta model describes the characteristics of the ejected particles after a kinetic impact and is used to generate the initial conditions of the propagation. The ejected particles are defined by their size, ejection location, ejection speed, and launch direction. The ejecta model is defined using a density function of the form [9]:

$$p(\mathbf{x}) = p(s, r, \xi, \psi) = p_s(s) \cdot p_\xi(\xi) \cdot p_{\psi|r}(\psi|r) \cdot p_r(r), \tag{4}$$

where s is the particle radius, r the ejection location (i.e., distance from the centre of the crater), ξ and ψ are the in-plane and out-of-plane ejection angles relative to a normal impact (i.e., an impact perpendicular to the surface of the target). A detailed description of the expressions of the different probability distribution functions can be found in [9, 10]. A strength of this distribution-based implementation of the ejecta model is that the distributions are analytical and can be easily sampled and integrated to generate the initial conditions of the propagation we need. Given these features, we can

Table 1 Asteroid 1998 KY26 properties [3, 4].

Quantity	Symbol	Value
Mean diameter (m)	d_a	30
Bulk density (g / cm^3)	ρ_a	2.8
Rotational period (min)	T_a	10.7
Albedo (-)	a	0.12

estimate the number of ejected particles for different ranges of ejection variables (s, r, ξ, and ψ) by integrating the distribution. In this way, assign "packets of particles" that we call *representative fragments* [9] to each sample in the distribution so that we can better monitor the evolution of ejecta plume as a whole. In fact, in the first approximation, propagating one sample translates into following a large amount of associated representative fragments.

C. Ballistic Limit Equations

Ballistic Limit Equations (BLEs) are semi-empirical relations that assess impact damages by projectiles impacting spacecraft surfaces [11]. In the literature, there exists a variety of BLEs, developed for single-wall and multiple-wall structures and for different materials, which allow a simplified, yet immediate understanding of the effect of an impact on the spacecraft. In this work, we utilise two kinds of BLEs. The first equation that models the particle interaction with a single-wall aluminium structure for low-speed impacts and has the following expression [11]:

$$d_c = \left[\frac{\frac{1}{K_{3S}} \cdot t_w^{0.5} \cdot \left(\frac{\sigma_y}{40}\right)^{0.5}}{0.6 \cdot \rho_p^{0.5} \cdot v_p^{2/3}} \right]^{\frac{18}{19}}, \tag{5}$$

where t_w is the thickness of the aluminium panel in cm, σ_y is the yield strength of the panel in ksi, ρ_p and v_p are the density and speed of the impacting particle in g cm^{-3} and km s^{-1}, respectively, and K_{3S} is a scaling constant whose value is 1.4 for impact on aluminium walls. This equation is used to model the effect on the structure wall and exterior panels. The second type of BLE is instead used for interaction with glass materials. This type of equation is used to assess the risk for the optical devices aboard Hayabusa2. The expression for the glass BLE is as follows:

$$d_c = \left[\frac{D_{c,\max}}{K \cdot \rho_p^{0.44} \cdot v_p^{0.44}} \right]^{\frac{3}{4}}, \tag{6}$$

where $D_{c,\max}$ is the maximum allowed crack diameter on the instrument glass in cm and K is a scaling constant that depends on the considered material (30.9 for *fused silica* and 15.1 for *fused quartz*).

III. Projectile Impact Simulations

By combining the dynamical model and the ejecta model we can study the motion of the particle around the asteroid and predict its fate. Since asteroid 1998 KY26 has a diameter of approximately 30 meters, its gravitational attraction is extremely weak causing only the very slow ejecta released from the crater to be influenced by its gravity field. The remaining portion of the ejecta plume will quickly escape from the sphere of influence of the asteroid ($\approx$ 115 m); however, their escape trajectory will be affected by the high spin rate of the asteroid. To study these aspects and to take into account the poorly known characteristics of 1998 KY26, we perform a sensitivity analysis on the impact location of the projectile and the characteristics of the soil of the asteroid. The characteristics of asteroid 1998 KY26 used for the present study are summarised in Table 1, while the characteristics of the projectile are summarised in Table 2.

A. Effect of the asteroid's soil cohesion

For this analysis, we consider different strength levels for 1998 KY26. Following the work of [14], we consider two reference values for the asteroid's cohesion: the least upper bound cohesion strength $C_{0\mathrm{L}}$ = 24.94 Pa and the required cohesion $C_{0\mathrm{U}}$ = 61.3 Pa. Both these values have been derived from analysing the necessary cohesion strength so that

Table 2 Impactor properties [12, 13]

Quantity	Symbol	Value
Speed (m/s)	U	300
Radius (mm)	a	8
Mass (g)	m	5

1998 KY26 is not torn apart by its very high rotational speed. We can immediately notice that the aforementioned values indicate that a very low cohesion is required for 1998 KY26. This means that even a small impact on its surface can lead to large cratering events, making it interesting to study possible future scenarios. Given the large uncertainties on the nature of the soil of 1998 KY26, we decided to use two additional values for the asteroid's cohesion. Specifically, a strength level 10 times and 100 times $C_{0\mathrm{U}}$, respectively, for a total of four different cases.

Figure 1 shows the effect of the four levels of asteroid cohesion on the resulting crater diameter, assuming a projectile with characteristics as in Table 2. The boxplot shows also the range of crater radius values within the 25% and 75% quartiles resulting from a sensitivity analysis varying values of the asteroid density of ±20% and the asteroid radius of ±10% to account for uncertainties in the characterisation of asteroid 1998 KY26. The results show a range of possible crater radii ranging from about 8 cm to about 30 cm, with uncertainties remaining contained for all possible values of strength. It is interesting to observe that despite the very small diameter of the projectile, a comparatively large crater could be generated and observed by the spacecraft.

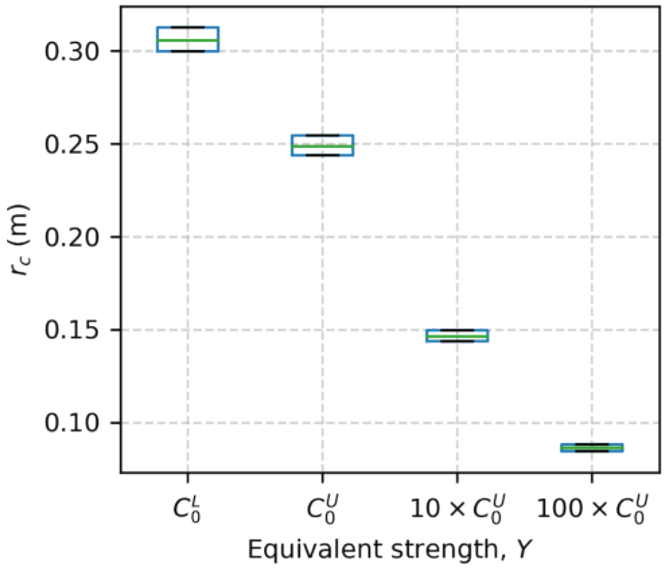

Fig. 1 Estimate of impact crater size as function of the cohesion level.

Following the analysis on the impact crater size, we performed a series of simulations to understand the motion of the ejected particles around the asteroid for a longer time span. Specifically, we simulated an impact with characteristics as in Table 2, sampling 500 000 samples from Eq. 4 and propagated them for one week assuming the dynamical environment as described in Section II.A. The impact simulation is repeated for the four levels of strength analysed and is assumed to happen on the north pole of the asteroid to eliminate the effect of the high spin-rate of 1998 KY26. In this way, it is possible to isolate the effect of the cohesion level on the fate of the generated ejecta. Figure 2 shows a summary of the aforementioned simulations. The blue line shows the fraction of particles re-impacting the asteroid after one week of simulation and as a function of the cohesion. Similarly, the orange line shows the fraction of particles that have escaped the Hill's sphere after one week. We can readily observe that, given the very low gravitational attraction of 1998 KY26, most of the particles escape the system. Indeed, almost all the particles ejected escape for the cases with $10 \times C_{0\mathrm{U}}$ and $100 \times C_{0\mathrm{U}}$, corresponding to 613 Pa and 6130 Pa, respectively. As expected, this analysis shows that most

of the fragments generated by the impactor release will quickly escape, unless the cohesion level of 1998 KY26 is close to its lower acceptable limit. In this case, between 10 and 15% of the particles may re-impact the asteroid.

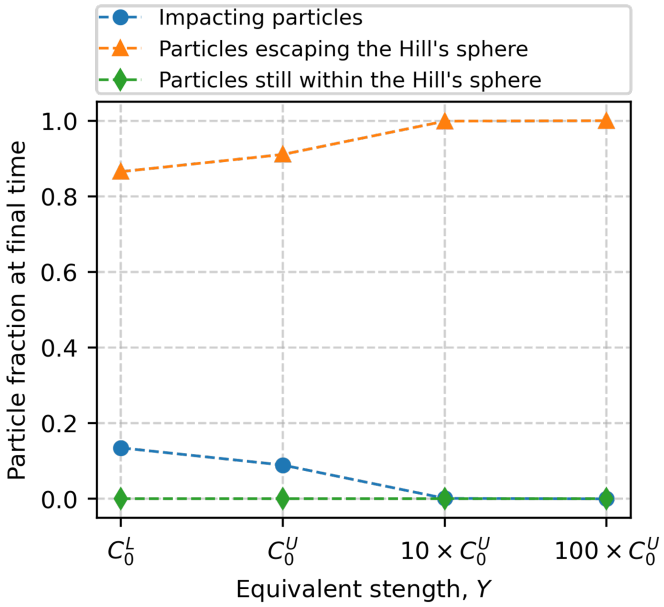

Fig. 2 Particle fraction at the final simulation time (one week) for four different strength levels. In blue the fraction of impacting particles, in orange the particles escaping the Hill's sphere, and in green the particles still within the Hill's sphere.

B. Effect of impact location

Following the analysis on the effect of the cohesion, we performed a similar analysis concerning the effect of the impact location. Given the high spin rate of 1998 KY26, the impact location may strongly influence the resulting dynamics of the ejected particles. Taking as a reference the previous results for a normal impact on the north pole of the asteroid (corresponding to 90 deg declination in the synodic reference frame), we varied the impact right ascension and declination to assess their effect on the overall dynamical evolution of the ejecta. We experimented with eight different cases, varying the right ascension from 0 deg to 360 deg with steps of 90 deg and two values of declination, 80 deg and 85 deg. We have decided to exclude lower declination as in those cases all the particles where directly escaping due to the high rotational contribution of the asteroid. The cohesion level for these simulations has been fixed to the second one, C_{0U} and the propagation time is again one week. Figure 3 shows the results after one week of simulation in terms of particle fractions for three different type of outcomes: impacting particles, particles escaping the Hill's sphere, and particles still within the Hill's sphere.

We can observe that the effect of the impact location is small but not negligible. As expected, the lower the declination, the lower the percentage of particles re-impacting is, given the higher contribution to the ejection speed from the rotation of the asteroid. However, for the cases with impact right ascension of 90 deg, we can observe a slightly higher percentage of impacting particles. This is the case where the contribution of the rotation of the asteroid combined with the ejection speed sends the ejecta towards the Sun. Given the small diameter of the particles, they are highly affected by solar radiation pressure (SRP); therefore, some of the particles that are ejected towards the Sun are eventually pushed back towards the asteroid by the SRP effect. We can observe this behaviour in Figure 4, where the evolution of the particles' density as a function of time after impact and altitude from the asteroid is shown. We can clearly observe that the highest amount of particles escape; however, we also observe that some of the particles do come back towards the asteroid after around 10 hours. These are mainly the smaller particles, which are mostly affected by SRP due to their higher area-to-mass ratios.

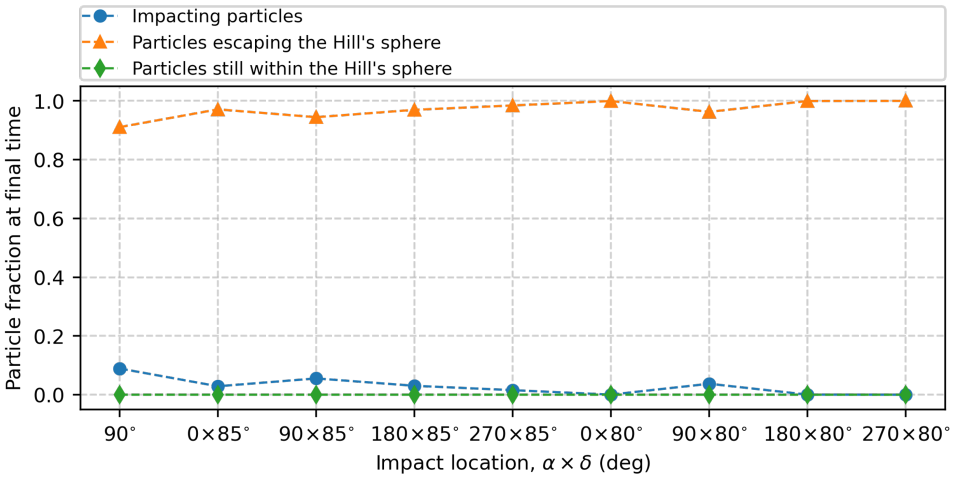

Fig. 3 Particle fraction as a function of the impact location.

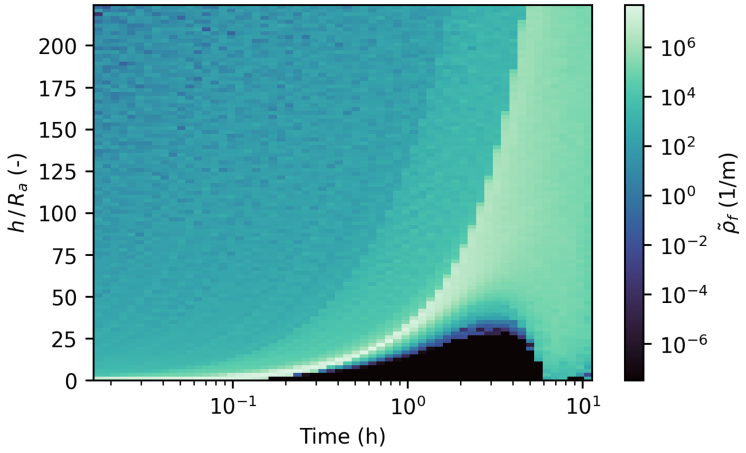

Fig. 4 Particle density evolution of time and altitude from the asteroid surface.

C. Ejecta trajectories performing multiple revolutions

Despite that the previous analyses have shown that the number of ejected particles still orbiting the asteroid after one week of simulation is very small, it is still interesting to analyse what happens to those particles. Therefore, we looked at the previous long-term simulations and checked the percentage of ejecta performing at least one pericentre passage (Figure 5). The results show that approximately 0.01% (about 4000 fragments) and 0.04% (about 9000 fragments) of the total number of particles exhibit such a behaviour for the cases with cohesion C_{0L} and C_{0U}, respectively. The other two cohesion cases show no presence of such orbits.

Therefore, there is the possibility for a few thousands fragments to still be orbiting 1998 KY26 after the projectile impact. It is then interesting to understand the characteristics of such fragments. Figure 6 shows the particle diameter and time-of-flight distributions for the multi-pass orbits. Figure 6a shows that most of the surviving fragments have a diameter around 1 cm, while Figure 6b shows that the time-of-flight is mostly above 12 hours, with several simulations reaching the end of the simulation (one week). This indicates that another small percentage of particles could still be orbiting for more than one week.

IV. Spacecraft-ejecta interaction and safety analysis

In this section, we assess the risk posed by the ejecta plume on the spacecraft during the projectile release operations. Specifically, we evaluate the impact probability on the spacecraft and the possible penetration probability for specific

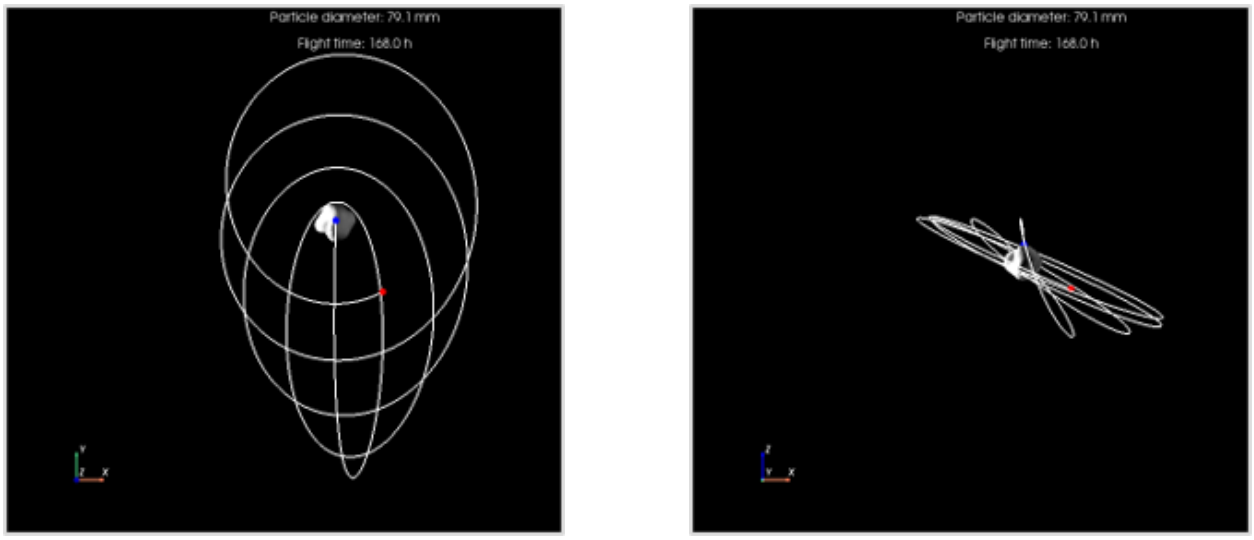

(a) **(b)**

Fig. 5 Example of orbit performing several pericentre passages. (a) projection along the x-y plane of the synodic reference frame (b) projection along the x-z plane of the synodic frame.

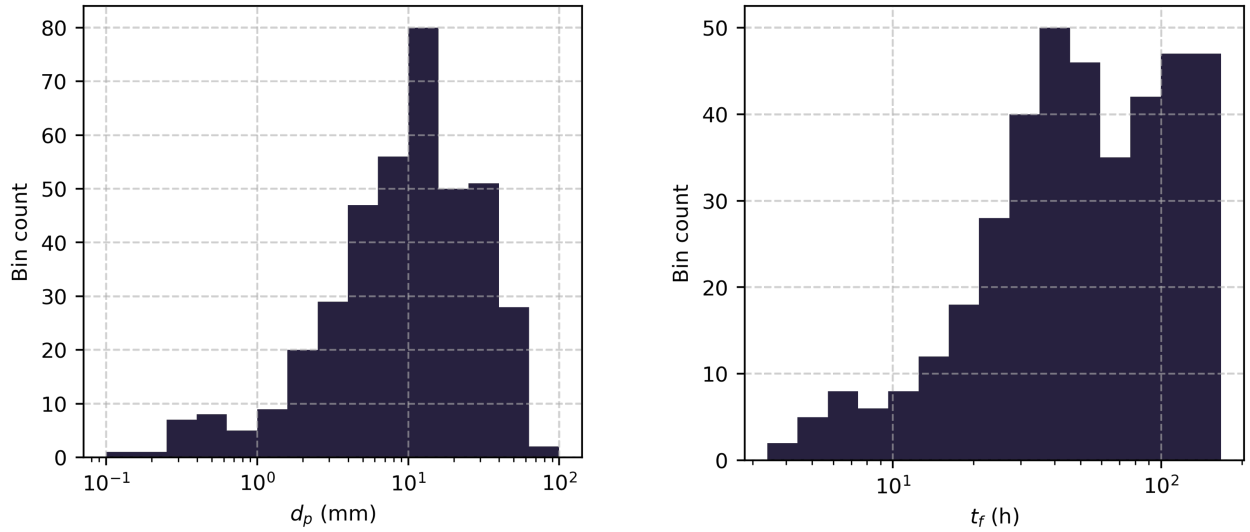

(a) **(b)**

Fig. 6 Distribution of the particle diameter (a) ad time-of-flight (b) for particles performing multiple pericentre passages.

surfaces types: a single-wall aluminium panel (which represents a structural panel of the spacecraft) and a glass-like material (which is representative of an optical instrument). To perform such analysis we first simplify the geometry of the problem as shown schematically in Figure 7a. The spacecraft is assumed to descend vertically during the projectile release operation and the projectile is released normally to the soil. Consequently, the resulting ejecta plume will be symmetrical with respect to the azimuth direction. Therefore, we reduce the analysis to a two-dimensional computation. To further simplify the computation and exploit the analytical formulation of the ejecta plume distribution (see Section II.B), we reduce the ejecta-spacecraft interaction to an ejecta-disk interaction, thus assuming the spacecraft surface can be represented by a disk enclosing the spacecraft span. Throughout these analyses, we have used a cohesion level equal to C_{0U} for the asteroid's soil.

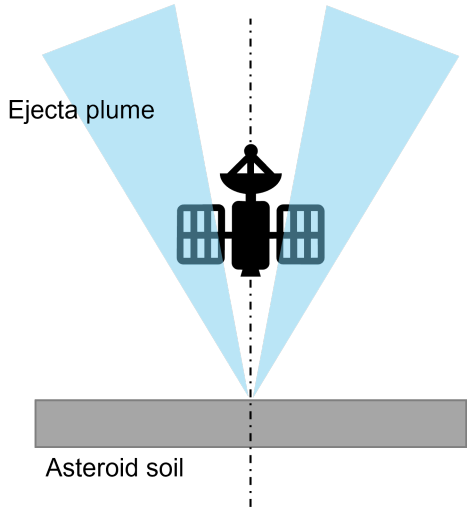

(a) Schematic representation of the ejecta plume interaction with the spacecraft.

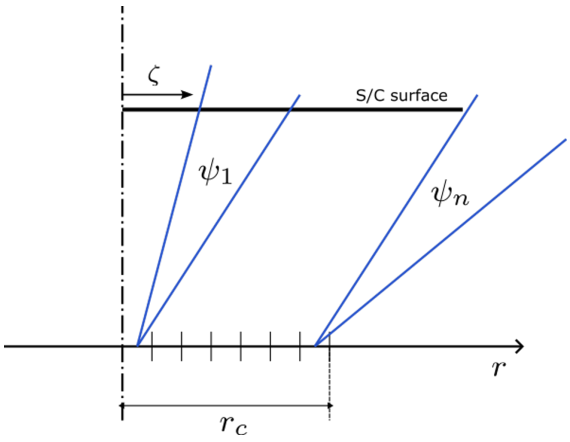

(b) Diagram of the mathematical model of the interaction between the out-of-plane ejecta plume distribution and the spacecraft.

Fig. 7 Schematics of the simplified approach to estimate the spacecraft-plume interaction and the resulting impact probability.

Because the problem is now two-dimensional, we can also reduce our ejecta distribution to the only two variables we need, the radius, r, and the out-of-plane ejection angle, ψ. In this case, the ejecta distribution has the following expression:

$$p_{\psi r} = p_{\psi|r} \cdot p_r \tag{7}$$

At this point, to find the impact probability we need to integrate Eq. 7 on a disk of radius $r_{S/C}$, representing the spacecraft envelope as shown schematically in Figure 7b. As the distribution of the out-of-plane ejection angle, ψ, depends upon the ejection location, r, the conditional $p_{\psi|r}$ will interact differently with the spacecraft for different ejection locations. Therefore, we discretise the ejection location in a series of intervals up to the crater radius in order to perform the integration. The resulting expression of the collision probability is as follows:

$$p_{\text{imp}} = \sum_{k=1}^{N} \left[p_r \left(r_k \leq r < r_{k+1} \right) \cdot \int_{\psi} p_{\psi|r}(\psi|\bar{r}_k) \mathrm{d}\psi \right], \tag{8}$$

where N is the number of subdivisions of the impact crater radius, $p_r \left(r_k \leq r < r_{k+1} \right)$ is the probability that the ejected particle is within the lower and upper range of the crater size bin, and $\bar{r}_k$ is the mean ejection radius of each bin. To ease the computation of the integral, it is also possible to perform the following variable substitution: $\psi = \arctan\left(\frac{h}{\zeta - \bar{r}_k}\right)$, where h is the altitude of the spacecraft from the soil and ζ is defined as in Figure 7b. In this way, the inner integral can be evaluated between 0 and the spacecraft half-span directly.

Figure 8a shows the result of the computation of the impact probability using Eq. 8 varying both the spacecraft half-span size and its altitude from the ground. We can observe that there is a fairly clear separation between the area of no impact probability (blue shade) and the one with 100% impact probability (yellow shade). Since the highest density of the ejecta plume is concentrated within ψ angles between 40 deg and 50 deg, depending on the spacecraft altitude, most of the fragments can be avoided. If we consider more specifically the half-span size of the Hayabusa2 spacecraft (red lines in Figure 8a), we observe that a safe release may be possible from altitudes above about 4 m. In practice, the dark blue region defines a minimum altitude after which the release of the projectile has a negligible risk. It is of course necessary to consider that this is a simplified analysis which does not account for possible deviations of the projectile from the normal and that the soil of the asteroid has specific properties; however, it gives an indication on the possibility of performing the projectile release safely.

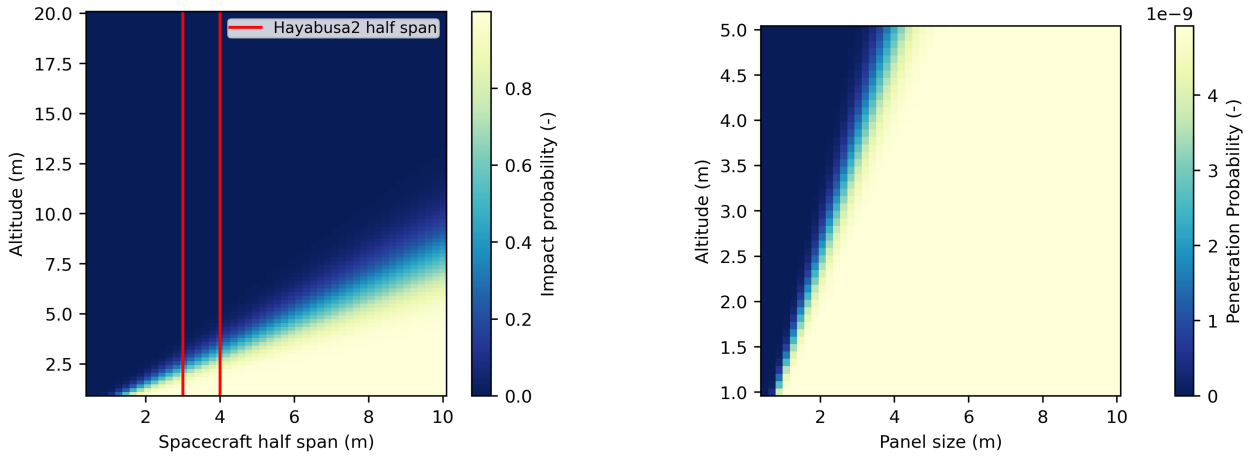

(a) Impact probability. **(b) Penetration probability.**

Fig. 8 Impact and penetration probability distribution for the ejecta plume impact with a single-wall aluminium panel.

Exploiting the computation of the impact probability, we also performed an analysis on the penetration probability. To do so, we combine the previous results with the probability distribution of the ejecta size [9]. Since the distribution of the particle size is considered independent from the other variables, we can directly compute it and multiply it inside Eq. 8 as follows:

$$p_{\text{imp}} = \sum_{k=1}^{N} \left[p_r \left(r_k \leq r < r_{k+1} \right) \cdot p_s \left(s > d_c/2; \bar{r}_k \right) \cdot \int_{\psi} p_{\psi|r}(\psi|\bar{r}_k) \mathrm{d}\psi \right], \tag{9}$$

where $p_s \left(s > d_c/2; \bar{r}_k \right)$ is the probability that the particle radius is greater than the critical radius (see Eq. 5). This value depends upon the ejection location because in the BLE that computes the critical diameter we need to provide the impact speed, which in turn depends on $\bar{r}_k$ [9]. Using this approach, we can compute the penetration probability on an aluminium wall of 1 mm thickness. Figure 8b shows such a result as a function of the release altitude. We can observe the same behaviour as in Figure 8a; however, in this case the penetration probability is negligible. Since the 1 mm thick panel on which we performed the analysis is a conservative assumption for a spacecraft exterior wall, we can conclude that the risk for the spacecraft structure to be penetrated by the impact ejecta is very low.

We then perform the same analysis on a more fragile material (glass-like) to assess the potential for cracking on optical devices. The approach is equivalent to the aluminium panel, the only change is represented by the different ballistic limit equation (Eq. 6). From this expression, we observe that the critical diameter is a function of the ejecta density (which we assume equal to the asteroid main body density), the ejecta speed, and the maximum allowed crack diameter on the glass, $D_{\text{c,max}}$. To perform this analysis, we specify three different allowed crack diameters: 1 µm, 10 µm, and 0.1 mm. The results of the analysis is shown in Figure 9. Figure 9a shows the crack formation probability as a function of the ejection location (because of the different ejection speed) and allowed maximum crack diameter. Initially all the curves for the three different $D_{\text{c,max}}$ follow the same increasing behaviour. This effect is due to the increase in number of particles having a diameter grater than the critical one. In fact, the further from the impact location, the greater is the number of particles ejected. At a certain point, however, the slope of the function changes for the larger $D_{\text{c,max}}$ values. This is an effect of the decreasing size of the critical diameter as the ejection location increases (due to the fact that the ejection speed decreases with the ejection location). Therefore, the slope of the curve will depend upon the rate at which the number of particles ejected increases and the ejection speed decreases as we increase the ejection location. The area underlying these distributions gives us the total crack formation probability for the three different $D_{\text{c,max}}$ values we are considering. Figure 9b shows these results. We can observe that for allowed crack sizes below 0.1 mm the crack formation is almost inevitable. Therefore, depending on the amount of damage that the optical instrument can sustain, it will be fundamental to try to limit the impact probability as much as possible during release by deploying the impactor from a sufficiently high altitude.

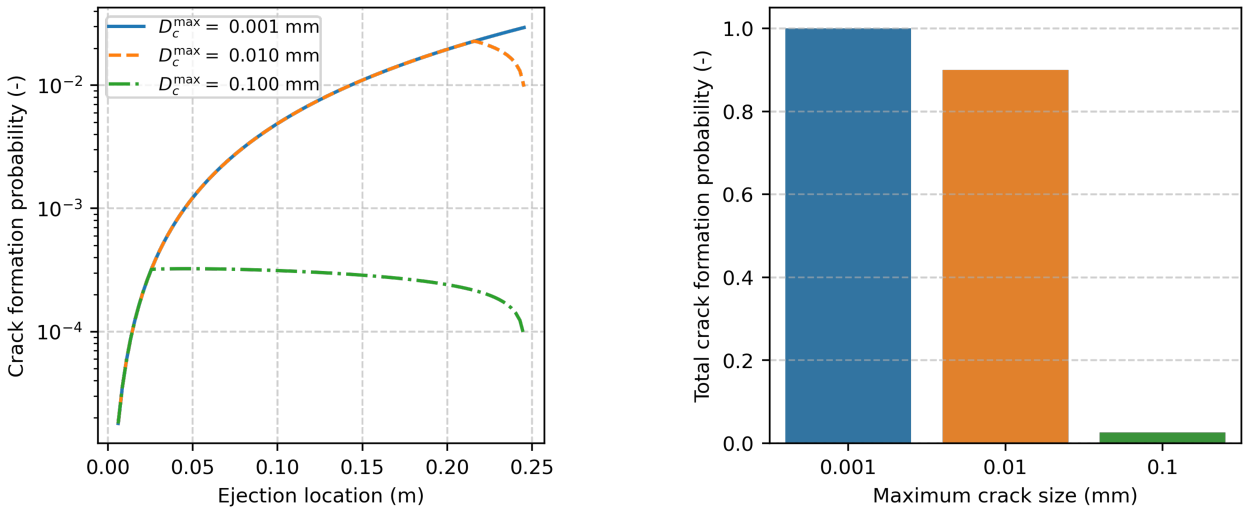

(a) Crack formation probability as a function of the ejection location for three different allowed crack sizes.

(b) Cumulative crack formation probability for three different allowed crack sizes.

Fig. 9 Crack formation probability for ejecta impact on glass material.

V. Conclusions and Discussion

In this work, we have carried out a preliminary analysis for the projectile release operations of mission Hayabusa2#. For these analyses, we studied the dynamical behaviour of the ejected fragments and assessed how they are affected by uncertainties in the asteroid's cohesion level and impact location. The analysis on the cohesion level revealed that only if 1998 KY26 cohesion is close to its physically possible minimum, some of the ejected fragments may re-impact or still orbit the asteroid after one week. In the other cases, all the particles will escape the sphere of influence. We also observed that a small percentage of the particles still orbiting may be trapped in long-lasting trajectories in which the particle performs several pericenter passages. We observed that these trajectories are more common for a cohesion level equal to C_{0U} and that the most probable particle size is in the order of 1 cm. Finally, we performed a risk analysis for the Hayabusa2 spacecraft during the projectile release operations. Making use of some simplifying assumptions, we reduced the problem of determining the impact and penetration probability on the spacecraft surface to the integral of a distribution over disk encompassing the spacecraft. From this statistical analysis, we were able to define a safe release region based on the combination of spacecraft size and altitude from the asteroid's surface. For the specific case of Hayabusa2#, a safety altitude of about 4 to 5 m was obtained. If the projectile is released above this altitude, the impact probability with the resulting ejecta will be negligible. However, in case the spacecraft is hit by some of the fragments, we also considered the possible damaging effects. We observed that for structural panels, such as aluminium, the penetration probability is negligible. However, for the glass parts of optical instruments the risk of crack formation can be very high. Depending on the minimum allowed crack size on the instrument, the probability of losing the instrument may be as high as 100% for allowed crack sizes of 1 µm.

Acknowledgments

This project has received funding from the European Union's Horizon 2020 research and innovation programme under the Marie Sklodowska-Curie grant agreement No 896404 - CRADLE. The authors acknowledge the financial support offered by the la Caixa Foundation (ID 100010434) under agreement LCF/BQ/AA20/11820034 to support the PhD studies of A.P.F.

References

[1] Yada, T., Abe, M., Okada, T., Nakato, A., Yogata, K., Miyazaki, A., Hatakeda, K., Kumagai, K., Nishimura, M., Hitomi, Y., et al., "Preliminary analysis of the Hayabusa2 samples returned from C-type asteroid Ryugu," *Nature Astronomy*, Vol. 6, No. 2, 2022, pp. 214–220. https://doi.org/10.1038/s41550-021-01550-6.

[2] Mimasu, Y., Kikuchi, S., Takei, Y., Saiki, T., Watanabe, S.-i., Tanaka, S., Hirabayashi, M., Sakatani, N., Kouyama, T., Yoshikawa, M., et al., "Extended mission of Hayabusa2," *Hayabusa2 Asteroid Sample Return Mission*, Elsevier, 2022, pp. 557–571.

[3] Kikuchi, S., Mimasu, Y., Takei, Y., Saiki, T., Scheeres, D. J., Hirabayashi, M., Wada, K., Yoshikawa, M., Watanabe, S.-i., Tanaka, S., et al., "Preliminary design of the Hayabusa2 extended mission to the fast-rotating Asteroid 1998 KY26," *Acta Astronautica*, 2023.

[4] Ostro, S. J., Pravec, P., Benner, L. A. M., Hudson, R. S., Sarounova, L., Hicks, M. D., Rabinowitz, D. L., Scotti, J. V., Tholen, D. J., Wolf, M., Jurgens, R. F., Thomas, M. L., Giorgini, J. D., Chodas, P. W., Yeomans, D. K., Rose, R., Frye, R., Rosema, K. D., Winkler, R., and Slade, M. A., "Radar and Optical Observations of Asteroid 1998 KY26," *Science*, Vol. 285, No. 5427, 1999, pp. 557–559. https://doi.org/10.1126/science.285.5427.557.

[5] Pedros-Faura, A., Trisolini, M., Tsuda, Y., Scheeres, D., Kikuchi, S., and McMahon, J., "Target Marker Deployment Strategies for Hayabusa2 Extended Mission to the Fast-Rotating Asteroid 1998 KY26," *34th International Symposium on Space Technology and Science*, 2023, pp. 1–10.

[6] Soldini, S., and Tsuda, Y., "Assessing the hazard posed by Ryugu ejecta dynamics on Hayabusa2 spacecraft," *26th International Symposium of Space Flight Dynamics*, 2017, pp. 1–11.

[7] Trisolini, M., Colombo, C., and Tsuda, Y., "Target selection for Near-Earth Asteroids in-orbit sample collection missions," *Acta Astronautica*, Vol. 203, 2023, pp. 407–420. https://doi.org/https://doi.org/10.1016/j.actaastro.2022.12.012.

[8] Villegas-Pinto, D., Soldini, S., Tsuda, Y., and Heiligers, J., "Temporary Capture of Asteroid Ejecta into Periodic Orbits: Application to JAXA's Hayabusa2 Impact Event," *AIAA Scitech 2020 Forum*, 2020, p. 0221.

[9] Trisolini, M., Colombo, C., and Tsuda, Y., "Ejecta cloud distributions for the statistical analysis of impact cratering events onto asteroids' surfaces: A sensitivity analysis," *Icarus*, Vol. 394, 2023, p. 115432. https://doi.org/https://doi.org/10.1016/j.icarus.2023.115432.

[10] Trisolini, M., Colombo, C., Tsuda, Y., et al., "Ejecta dynamics around asteroids in view of in-orbit particle collection missions," *72nd International Astronautical Congress (IAC 2021)*, 2021, pp. 1–10.

[11] Shannon, R., and Christiansen, E., "Micrometeoroid and Orbital Debris (MMOD) Shield Ballistic Limit Analysis Program," , 2009.

[12] Saiki, T., Imamura, H., Arakawa, M., Wada, K., Takagi, Y., Hayakawa, M., Shirai, K., Yano, H., and Okamoto, C., "The small carry-on impactor (SCI) and the Hayabusa2 impact experiment," *Space Science Reviews*, Vol. 208, 2017, pp. 165–186.

[13] Sawada, H., Okazaki, R., Tachibana, S., Sakamoto, K., Takano, Y., Okamoto, C., Yano, H., Miura, Y., Abe, M., Hasegawa, S., et al., "Hayabusa2 sampler: collection of asteroidal surface material," *Space Science Reviews*, Vol. 208, 2017, pp. 81–106.

[14] Li, X., and Scheeres, D. J., "Analysis of cohesion in fast-spinning small bodies," *The Planetary Science Journal*, Vol. 2, No. 6, 2021, p. 229.